

## SOFTWARE

# eXamine: a Cytoscape app for exploring annotated modules in networks

Kasper Dinkla<sup>1†</sup>, Mohammed El-Kebir<sup>2,3†</sup>, Cristina-Iulia Bucur<sup>2,3</sup>, Marco Siderius<sup>3</sup>, Martine J. Smit<sup>3</sup>, Michel A. Westenberg<sup>1\*</sup> and Gunnar W. Klau<sup>2,3</sup>

\*Correspondence:

[m.a.westenberg@tue.nl](mailto:m.a.westenberg@tue.nl)

<sup>1</sup>Eindhoven University of Technology, Den Dolech 2, 5600 MB, Eindhoven, The Netherlands  
Full list of author information is available at the end of the article  
<sup>†</sup>Equal contributor

## Abstract

**Background:** Biological networks have growing importance for the interpretation of high-throughput “omics” data. Statistical and combinatorial methods allow to obtain mechanistic insights through the extraction of smaller subnetwork modules. Further enrichment analyses provide set-based annotations of these modules.

**Results:** We present eXamine, a set-oriented visual analysis approach for annotated modules that displays set membership as contours on top of a node-link layout. Our approach extends upon Self Organizing Maps to simultaneously lay out nodes, links, and set contours.

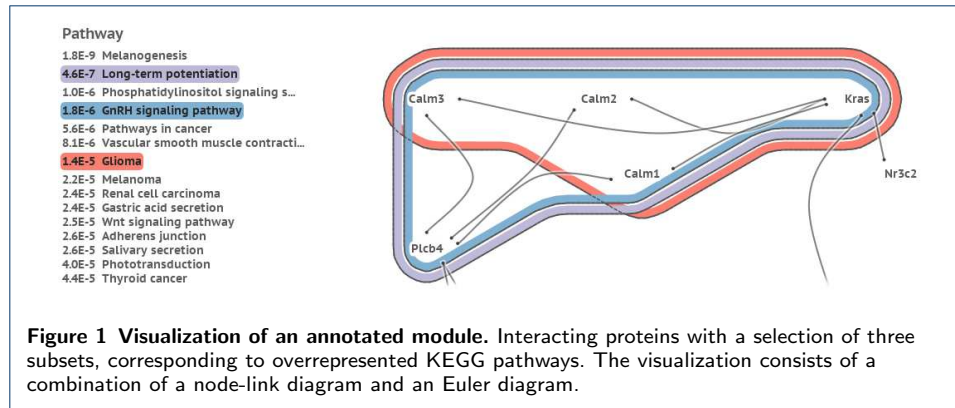
**Conclusions:** We implemented eXamine as a freely available Cytoscape app. Using eXamine we study a module that is activated by the virally-encoded G-protein coupled receptor US28 and formulate a novel hypothesis about its functioning.

**Keywords:** Network; Module; Set-based annotation; Visualization; Cytoscape; Self Organizing Maps; Network analysis

## Background

Traditionally, computational approaches to analyze high-throughput “omics” data have been *gene-centric* and typically result in ranked lists of differentially expressed genes [1–3]. Later, gene-centric approaches have been complemented by *pathway-based* [4, 5] and *network-based* methods [6, 7]. While pathway-based approaches identify overrepresented pathways from databases such as the Kyoto Encyclopedia of Genes and Genomes (KEGG) [8], network-based approaches yield small, *de novo* subnetwork modules that may span several pathways taking their crosstalk into account [9]. To assess the significance of such a module, a subsequent overrepresentation analysis is performed to identify enriched categories originating from ontologies such as the Gene Ontology (GO) [10] or enriched pathways from KEGG [8]. This results in an *annotated module*, which, in addition to its network structure, captures the enrichment information using a *set system*, that is, a family of possibly overlapping sets of nodes—see Figure 1 for an illustration. The interpretation of annotated modules can be facilitated using visualization techniques.

There are many tools for interpreting and exploring biological networks [11], including the popular open source platforms Cytoscape [12] and PathVisio [13]. However, they currently provide only limited capability to visualize annotated modules. PathVisio is a pathway analysis approach, where sets are restricted to subsets of



static, pre-defined individual pathways and set membership is shown by node colors. Cytoscape's group attributes layout can be used to visualize partitions by showing disjoint parts in separate circles, but does not support overlapping sets. The Venn and Euler diagram app<sup>[1]</sup> for Cytoscape does support overlapping sets, but their number is limited to four. In this app, network and sets are visualized separately: set membership is conveyed by selecting a set and its corresponding nodes are highlighted in Cytoscape's network view (see Figs. 9a and 9b). The RBVI collection of plugins<sup>[2]</sup> facilitates creation and editing of Cytoscape groups, and provides a group viewer that relies on aggregation of groups into meta-nodes. These meta-nodes can be visualized as standard nodes, as nodes containing embedded networks, or as charts. This approach, however, does not allow for visualization of overlapping sets.

In the information visualization field, *Euler diagrams* are used for an intuitive visualization of set systems [14–16], where items belonging to the same set are denoted by contours. Variants of these approaches visualize sets over items with predefined positions, e.g., over a given node-link visualization of a network. These methods range from connecting these items by simple lines (LineSets) [17], via colored shapes that are routed along the items (Kelp Diagrams) [18] and contours around the items (BubbleSets, see Fig. 9c) [19,20] to hybrid approaches (KelpFusion) [21]. Visualizing an annotated module, however, requires an integrated layout of both its network and set system topologies, which is not possible with these existing approaches. Euler diagram methods focus on the layout of the set relations at the expense of the network topology. Likewise, laying out the network first before superimposing set relations will emphasize network topology to the detriment of the set system. There exist some techniques that provide such integrated layouts [22–24], but they assume constraints on the network and set system topologies, e.g., strict partitions and no overlapping sets, and are therefore not applicable to our problem.

In this paper, we present a visual analysis approach designed around the typical characteristics of annotated network modules: (i) small and sparse network topology, with nodes and edges that number in the dozens; (ii) large set system, where sets outnumber edges and vary in size, overlap, and distribution of set member nodes across the network. Our approach displays sets as contours on top of a node-link layout, however, in contrast to previous work mentioned above, our approach

[1] <http://apps.cytoscape.org/apps/vennandeulerdiagrams>

[2] <http://www.rbvi.ucsf.edu/cytoscape/groups/>

places emphasis on the interactive exploration of a large set system together with an underlying network topology, see Fig. 1. We do this in a unified way using *Self Organizing Maps* (SOMs)—also known as Kohonen maps. SOMs map high-dimensional data to discretized low-dimensional space [25] and have successfully been applied to lay out networks [26]. We have implemented this approach as a generic Cytoscape app eXamine, such that it can be applied to annotated network modules as they appear for various domain-specific networks.

We apply eXamine to study an annotated module that is activated by the virally-encoded G-protein coupled receptor US28. We obtained the module by analyzing microarray expression data of US28 vs. mock transfected murine cell lines within the context of a network consisting of murine signaling and metabolic pathways from KEGG. The annotation consists of enriched GO-terms and KEGG pathways as well as gene expression fold changes. Using eXamine, we formulate a novel hypothesis about deregulated signaling of  $\beta$ -catenin by the viral receptor protein US28.

## Method and Implementation

Visualizing an annotated module amounts to visualizing a *hypergraph* consisting of binary edges, representing the network structure, and  $n$ -ary edges, representing the set system on the nodes. As opposed to combining multiple existing techniques—e.g., a force simulation to position the nodes according to the binary edges [27], a node overlap removal algorithm to keep nodes identifiable [28], and subsequent construction of a density field to derive contours for  $n$ -ary edges [19]—our approach uses a single technique for both visualization tasks. To this end, we assign a bit vector  $\mathbf{t} = (t_1, t_2, \dots, t_M)$  to every node  $t \in V$  (the set of nodes in the annotated module) that encodes its membership in binary and  $n$ -ary edges  $S_1, S_2, \dots, S_M$ . That is,  $t_i = 1$  if  $t \in S_i$  and  $t_i = 0$  if  $t \notin S_i$ .

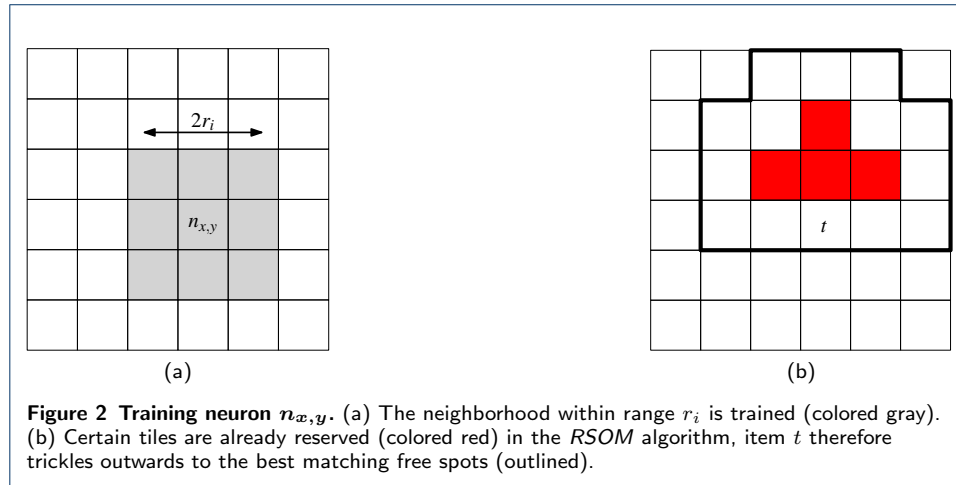
To make this representation more concrete, consider the annotated module shown in Fig. 1. The nodes are represented as the set  $V = \{\text{Calm1}, \text{Calm2}, \text{Calm3}, \text{Kras}, \text{Nr3c2}, \text{Plcb5}\}$ . There are seven sets representing the edges and three sets representing pathway memberships. The edge sets are  $S_1 = \{v_1, v_4\}$ ,  $S_2 = \{v_1, v_6\}$ ,  $S_3 = \{v_2, v_4\}$ ,  $S_4 = \{v_2, v_6\}$ ,  $S_5 = \{v_3, v_4\}$ ,  $S_6 = \{v_3, v_6\}$ , and  $S_7 = \{v_4, v_5\}$ . Note that nodes  $v_4$  (Kras) and  $v_6$  (Plcb4) have some additional outgoing edges, but their targets are not visible in the image. Therefore, we ignore these edges in this example. The pathway memberships are the Glioma set  $S_8 = \{v_1, v_2, v_3, v_4\}$ , the Long-term potentiation set  $S_9 = \{v_1, v_2, v_3, v_4, v_6\}$ , and the GnRH signaling pathway set  $S_{10} = \{v_1, v_2, v_3, v_4, v_6\}$ . Now, for example, node  $v_5$  gets assigned the bit vector  $\mathbf{t}_{v_5} = (0, 0, 0, 0, 0, 0, 1, 0, 0, 0)$ , and node  $v_6$  the bit vector  $\mathbf{t}_{v_6} = (0, 1, 0, 1, 0, 1, 0, 0, 1, 1)$ .

This high-dimensional representation is then used to lay out the nodes without overlap, the binary edges as curves and the  $n$ -ary edges as contours.

### Extension to Self Organizing Maps

Self Organizing Maps (SOMs), introduced by Kohonen [25], are an artificial neural network that are used to map high-dimensional data items to discretized low dimension. In a visualization setting SOMs are used to cluster similar items together in a 2D embedding, creating a landscape of items based on their features [29, 30].

Typical SOMs consist of a square grid of size  $N \times N$  with a neuron  $n_{x,y} \in [0..1]^M$  at every grid cell. A neuron  $n_{x,y}$  is a bit vector of size  $M$  whose dimension matches the data items' dimensions. In our case the data items  $\mathbb{T}$  correspond to the set of nodes  $V$  in the annotated module. The training algorithm applies unsupervised reinforcement learning in an iterative fashion: at every iteration  $i \in \{1, \dots, I\}$  all data items  $t \in \mathbb{T}$  are considered and the neuron that matches  $t$  most closely is determined using a distance function such as the Euclidean or Manhattan norm. This neuron and its neighboring neurons within radius  $r_i$  are updated to match  $t$  even more closely by setting their respective vectors  $q$  to  $q + \alpha_i(t - q)$ —see Fig. 2(a). In early iterations  $i$ , the trained neighborhoods are large with  $r_i$  close to the grid size  $N$  and the training strength  $\alpha_i$  close to 1. The parameters  $r_i$  and  $\alpha_i$  decrease monotonically with increasing  $i$ . As such, items that differ strongly will distribute across the map to establish their own regions in the grid at early stages. Items with smaller differences are separated along the grid at a more local level as the training iterations progress.



**Reservation based training.** The drawback of standard SOMs is that similar items may end up at the same grid position. Usually this is solved by showing aggregate depictions of items, but in our case we want to have separate depictions without overlap. Therefore, each item has to map to a unique grid position. We achieve this by altering the training algorithm:

**Algorithm RSOM( $\mathbb{T}$ )**

1. **for**  $i \leftarrow 1$  **to**  $I$
2.     **do** Initialize copy  $\mathbb{U}$  of  $\mathbb{T}$  and clear neuron reservations.
3.     **while**  $\mathbb{U}$  contains items
4.         **do** Draw and remove item  $t$  from  $\mathbb{U}$ .
5.         Find unreserved neuron  $n_{x,y}$  with smallest distance  $d(t, n_{x,y})$ .
6.         Reserve  $n_{x,y}$  for  $t$ .
7.         **for** any neuron  $q$  within range  $r_i$  from  $(x, y)$
8.             **do**  $q \leftarrow q + \alpha_i(t - q)$

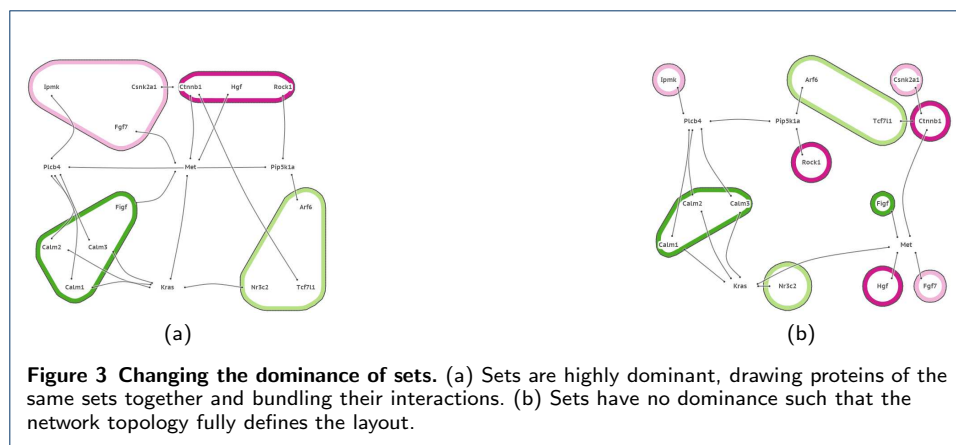
Now items are actively assigned to a unique neuron after every training iteration because once a neuron is reserved by an item, subsequent items will ignore it. This

causes a flooding effect where similar items end up in the same area of the grid and trickle outwards as the area becomes more crowded—see Fig. 2(b).

**Configuration.** As the distance function  $d$  we use the metric distance form of cosine similarity, i.e.  $d(q, p) = \cos^{-1}((q \cdot p) / (|q||p|))\pi^{-1}$ . For our data items this measure performs better than the Euclidean and Manhattan norms. We train the SOM with a learning strength and neighborhood range that decrease linearly with increasing iteration  $i$ , i.e.  $\alpha_i = 0.01 \cdot (1 - i/I)$  and  $r_i = \lfloor (1 - i/I) \cdot N \rfloor$ . As for the number of neurons and iterations we use  $N = 2|\mathbb{T}|$  and  $I = 10^5/|\mathbb{T}|$ , respectively. Instead of using a square tiling of the neurons, we use a hexagonal topology as it results in improved set contour aesthetics.

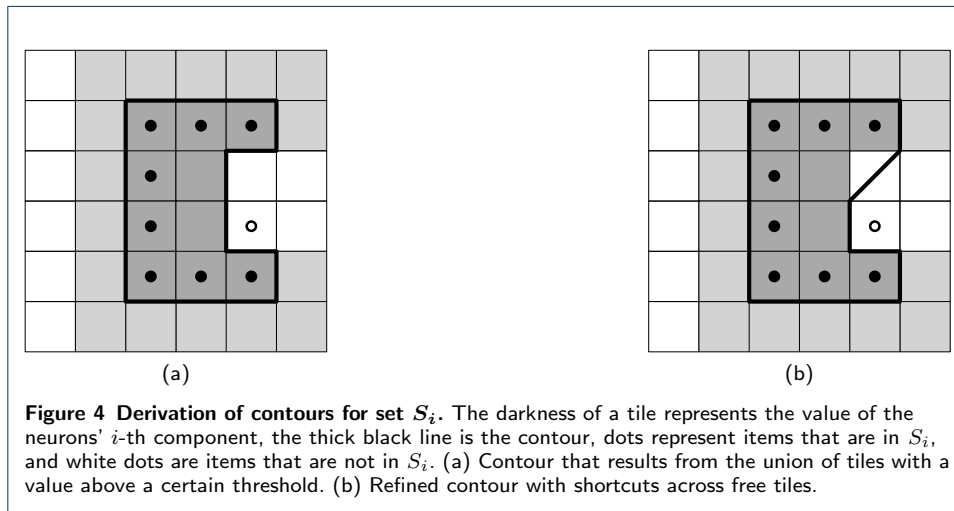
**Layout preservation.** Whenever the user selects or deselects a set, a new layout has to be computed. In order to preserve the user’s mental map, the new layout should change only slightly in comparison to the old layout. We achieve this by creating a new SOM and using the old layout as the initial configuration of the neurons, i.e., an item that was positioned at  $n_{x,y}$  in the old SOM is placed at  $n_{x,y}$  in the new SOM and its neighborhood is trained according to the new bit vector of the item. We ensure that the new SOM retains the starting configuration as much as possible by starting the training factor  $\alpha_i$  at value 0.01. Naturally, this imposes a trade-off between layout quality and conservation.

**Set dominance.** We allow the user to make a certain set more dominant in the layout by having the training algorithm place the items of that set closer to each other than the items of other sets. We do this by weighing the components of the item bit vectors: every  $S_i$  is given a weight  $w_i$  where initially  $w_i = 1$ . The bit vectors are subsequently augmented to incorporate these weights:  $t_i = w_i$  if  $t \in S_i$  and  $t_i = 0$  if  $t \notin S_i$ . The bit vector component of  $S_i$  will therefore play a more prominent role in distance metric  $d$  when the user increases  $w_i$ —see Fig. 3.



**Contours.** We use the SOM’s neuron grid to define the contours representing the active set system. Let  $S_i$  be an active set. The corresponding  $i$ -th components of the neurons define a scalar field that essentially is a fuzzy membership landscape

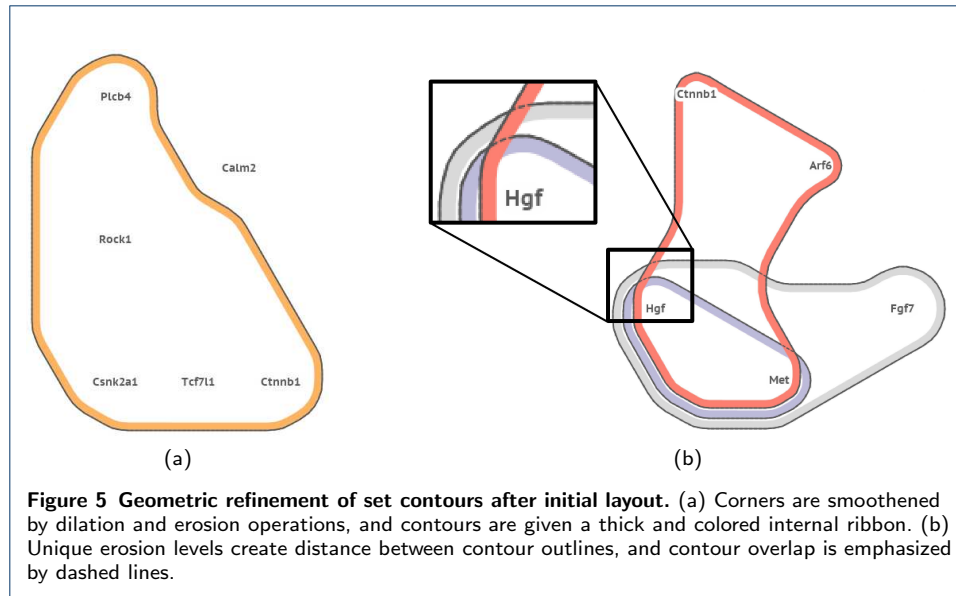
for  $S_i$ . This field is similar to the density field used in Bubble Sets [19]. Now, the inclusion of the grid tile of neuron  $n$  in the contour body is determined by imposing a threshold, of for example  $\frac{1}{2}$ , on the  $i$ -th component (see Fig. 4(a)). The contour can then be tightened to reduce sharp corners by including parts of tiles that are free of items, as illustrated in Fig. 4(b).



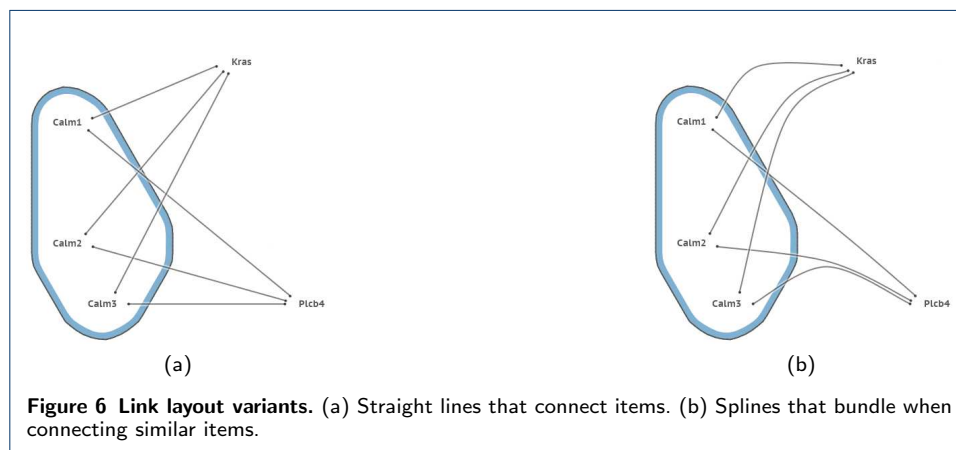
After establishing the layout of the contours, we apply geometric post processing [18] to improve aesthetics. We round the sharp corners of the initial layout by a dilation of  $r$ , erosion of  $2r$ , and subsequent dilation of  $r$ —see Fig. 4. Here *dilate* and *erode* are equivalent to *Minkowski sum* and *Minkowski subtraction* operators with a circle of radius  $r$  [31]. In addition, we nest the contours by applying different levels of erosion, enforcing a certain distance between them. We obtain the thick colored ribbons in Fig. 5 by taking the body  $b$  of a contour, eroding it to get a smaller body  $b_e$ , and taking the symmetric difference  $b - b_e$  of  $b$  and  $b_e$ —effectively cutting  $b_e$  out of  $b$ . We bound radius  $r$ , i.e., the extent of the erosions and dilations, by a fraction of the grid's tile size such that: no items end up being covered by a smoothed contour of  $S_i$  while not being part of  $S_i$ , and no contour sections of  $S_i$  are smoothed out while covering items that are part of  $S_i$ .

We draw the contours in the order of their nesting caused by their different erosion levels; the largest contour is drawn first and the smallest contour last. We assign the contour ribbons unique colors per set and draw them fully opaque to prevent any confusion caused by blended colors. We mitigate occlusion by limiting the width of the ribbons. Moreover, we draw the contours a second time as dashed lines such that occluded contour sections can be inferred—see Fig. 5(b).

**Links.** Instead of drawing edges as straight lines (see Fig. 6(a)), we use the SOM's neuron grid to bundle links. We do this by drawing a spline between two nodes along three control points [32]. These control points are derived by first linearly interpolating between the two nodes in the high-dimensional space that describe their set memberships, and then projecting the high-dimensional control points to the 2D space of the neuron grid. This projection is based on inverse distance weighting of the neuron's positions, using Shepard's method [33] with distance function  $d$  for the



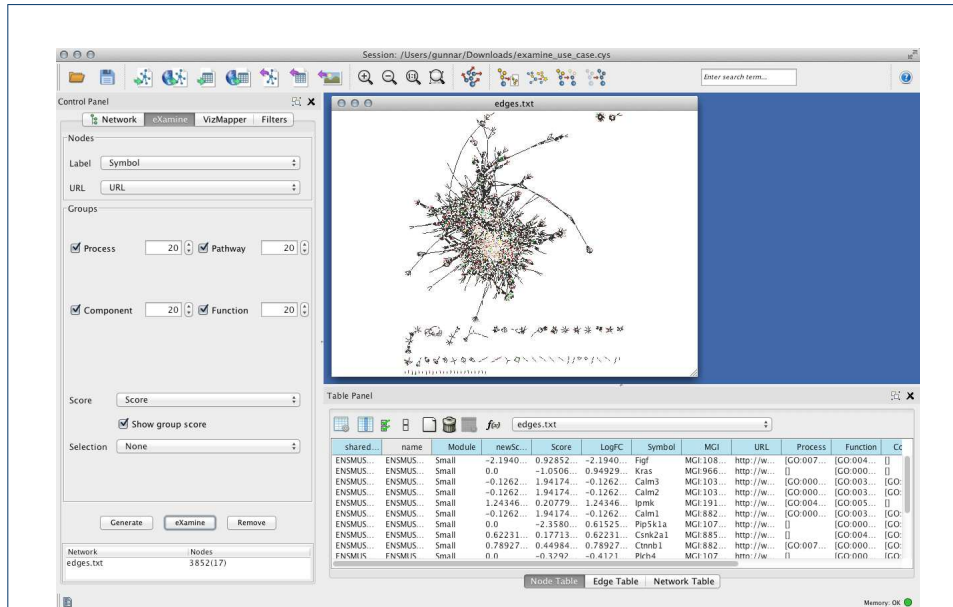
weighting. This gives those neurons closest to a control point, according to  $d$ , most influence on the control point's 2D position, resulting in a continuous mapping from the high-dimensional space of the items to the 2D layout space. Hence, the link  $(s, t)$  is guided by the neurons as it moves from node  $s$  to  $t$ . No routing is performed to prevent node and link intersections, nor does the described bundling approach suppress these situations. Instead, we avoid ambiguous situations by terminating links at ample distance from the nodes that they connect and marking their terminations with dots.



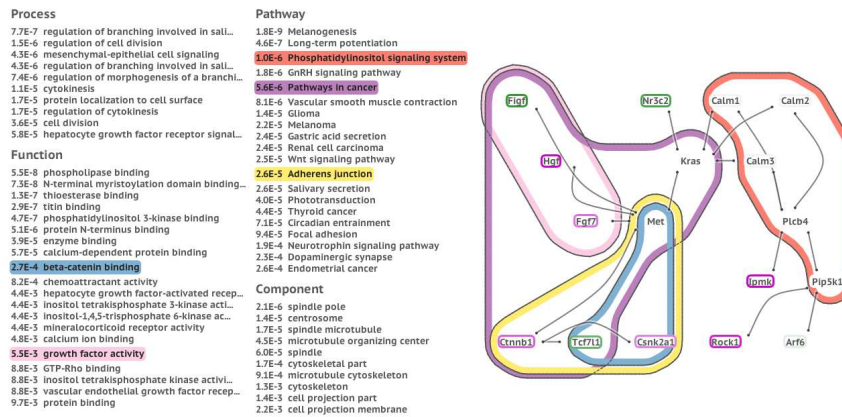
### Implementation

We implemented the described technique in a Cytoscape app with a design that emphasizes simplicity of interaction and visual presentation. The available sets are listed in the *set overview* on the left, where the user may select sets for inclusion in the annotated *network visualization* to the right—see Fig. 7.

We use Java's default graphics API to render the presented visualizations. Geometric operations on the contours, such as dilations and erosions, are performed via



(a)



(b)

**Figure 7 Overview of eXamine.** (a) In the eXamine control panel the user can choose which categories to visualize. (b) eXamine presents an overview of available sets at the left and the annotated module visualization at the right. Here, the GO terms *beta-catenin binding* and *growth factor activity*, and KEGG pathways *Phosphatidylinositol signaling*, *Pathways in cancer*, and *Adherens junction* are selected for inclusion as sets in the network view. Sets are assigned unique colors, where the set overview serves as a legend. Gene expression (log fold change) is visualized via superimposed rectangles on the text labels, integrating the attribute color mapping functionalities of Cytoscape.

Java Topology Suite [34]. All described functionalities can be used at interactive speeds for networks up to dozens of nodes, edges, and active sets, including the laying out of the network with the *RSOM* training algorithm.

**Interaction.** Interactions consist of simple mouse actions (see the video in the Supplemental Material). The inclusion of a set in the network visualization is toggled via the set's label in the set overview or its contour in the network visualization. Additional information about a set or node may be obtained via a hyperlink to a web page provided in the input data. This approach keeps the tool flexible, i.e., the tool itself does not have to be altered every time a new kind of set or node from a different database is loaded. The links of a node are emphasized when it is hovered over (see Fig. 8(a)) such that its direct neighborhood can be discerned from its surroundings. Moreover, sets that contain the hovered node are highlighted as well. Vice versa, the contours of a set are emphasized and its comprising nodes are highlighted when it is hovered over (see Fig. 8(b)). This provides immediate feedback to the user about node-set relations without having to select a set and consequently changing the layout of the network visualization.

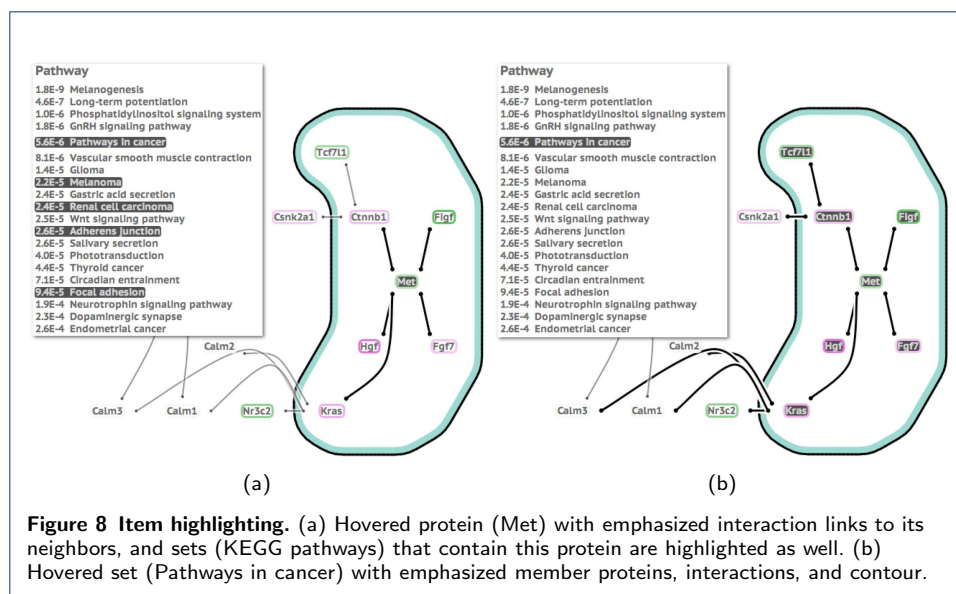


**Figure 8 Item highlighting.** (a) Hovered protein (Met) with emphasized interaction links to its neighbors, and sets (KEGG pathways) that contain this protein are highlighted as well. (b) Hovered set (Pathways in cancer) with emphasized member proteins, interactions, and contour.

The user can adjust the dominance of a set by hovering over either the set's label in the set overview or set's contour in the network visualization, and subsequently spinning the mouse wheel. This enables the user to give a set a central role in the layout (see Fig. 3(a)) or to remove any of its influence (see Fig. 3(b)). All changes to the visualization caused by interaction are animated. Colors and positions of items are altered gradually. Link layout changes are animated by the interpolation of their control points, while contour layouts are handled by fading out the old contour and fading in the new contour. The use of layout preservation, as described previously, in combination with animations helps to preserve the user's mental map.

**Color.** We assign selected unique, distinguishable colors derived from Color Brewer palettes [35] in a cyclic manner so as to avoid the consecutive assignment of the same

color. In addition, we avoid large differences in contrast. For example, we color text and set outlines dark gray instead of black in order to reduce their visual dominance. We only use intense black colors when items are hovered over or highlighted such that they attract attention, as shown in Fig. 8. Moreover, we emphasize labels of selected sets (in the set overview) with a more intense black color, retaining their legibility in a colored surrounding. Node labels have a white background to make sure that their text is legible when drawn on top of a set ribbon with a dark color. Likewise, links have halos that make them easier to distinguish and their intersections more pronounced.

**Cytoscape integration.** eXamine is tightly integrated into Cytoscape. We use Cytoscape's group functionality to represent sets and rely on the table import functionality for importing both the set and node annotations. We allow the user to group sets into different categories. We use the node fill color map attribute to color the node labels in eXamine. The user can invoke eXamine on the currently selected nodes via the eXamine control panel. There the user can select which categories to show as well as the number of sets per category. In addition, the user can specify that the Cytoscape selection should be updated to match the union or intersection of the selected sets in eXamine—see Fig. 7.

## Results and Discussion

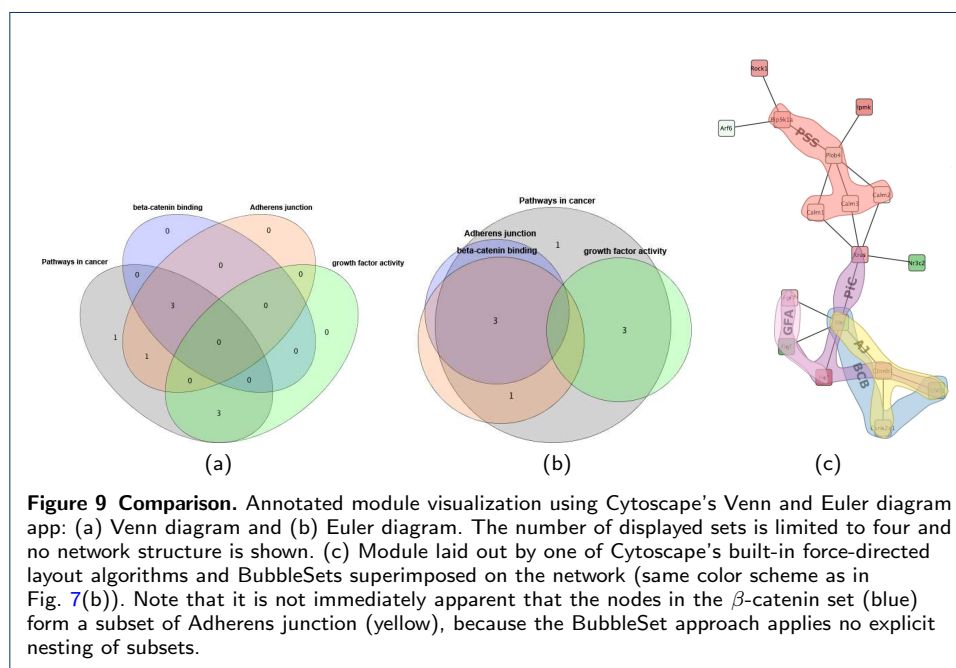
We will demonstrate how a domain expert can use eXamine by working out a case study in which we re-analyze a data set that some of the co-authors have studied extensively.

### Case study of US28-mediated signaling in Human Cytomegalovirus

We demonstrate our approach by a case study involving the Human Cytomegalovirus (HCMV), a specific type of herpes virus with a high incidence rate of 60% among humans [36]. Infection with HCMV in immune-competent individuals usually does not result in any symptoms. However, in immune-compromised patients the virus is correlated with pathologies such as hepatitis and retinitis [37]. Although not considered an oncogenic virus, HCMV components have been detected in various tumors, giving rise to the hypothesis the virus may act as an oncomodulatory factor in onset and development of cancer [38–40]. The high levels of latent infection and the potential role in pathology of the HCMV virus partly are associated with the HCMV-encoded G protein-coupled receptors (GPCRs). Of these viral GPCRs, US28 is most studied and is characterized as a chemokine sink [41]. Moreover, US28 is a promiscuous, constitutively active viral GPCR, which hijacks the host cell's signaling pathways and stimulates proliferative, anti-apoptotic responses interfering with natural programmed cell death [42–46]. In previous studies, we performed transcriptome analysis to evaluate US28-mediated pathways involved in pathological signaling. So far, a gene-centric approach was used to identify differentially regulated genes involved in HCMV-mediated pathology [44, 45].

In order to further identify the potential signaling properties associated with US28, we used eXamine to analyze the same data overlaid on the KEGG mouse network [8]. The overlaid input network consisted of 3863 nodes and 29293 edges.

We computed  $p$ -values reflecting whether a gene is significantly deregulated using RMA [47] and LIMMA [48]. By running Heinz [7], a tool for identifying deregulated modules, we obtained a deregulated module of 17 proteins. We performed an enrichment analysis to determine enriched GO-terms and KEGG pathways. Fig. 7 shows the identified module—the steps taken for obtaining this visualization are given in the Supplemental Text. Parts of the same module are visualized using Cytoscape’s Venn and Euler diagram app in Fig. 9a and 9b. The network structure is not shown in this visualization and the number of displayed sets is limited to four. Fig. 9(c) shows the module laid out by one of the built-in force-directed layout algorithms of Cytoscape. All five sets (see Fig. 7 for the color scheme) are shown as BubbleSets. The structure of the sets is not easy to understand: the nodes belonging to the  $\beta$ -catenin binding set (blue shape) form a subset of the Adherens junction set (yellow shape). Yet, BubbleSets does not show these two shapes as nested structures.

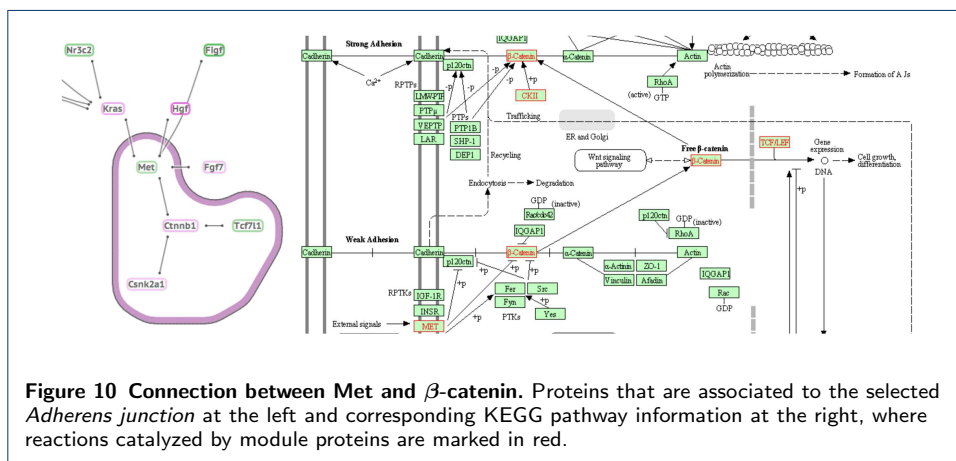


We start by obtaining a global overview of the module by considering the significantly enriched KEGG pathways. In line with the proposed oncomodulatory role of US28, the module shows significant enrichment for ‘Pathways in cancer’ (purple contour in Fig. 7). In addition, the identified module is significantly enriched for ‘Phosphatidylinositol signaling’ (red contour), which corresponds to previous work linking US28 to PLC-mediated calcium responses [42, 49].

Next, we focused on the ‘Pathways in cancer’ submodule. By hovering over Tcf711, Csnk2a1 and Met, we could see that these proteins are enriched for the GO-term ‘beta-catenin binding’. By looking at the expression color coding, we can see that  $\beta$ -catenin (Ctnnb1) and Csnk2a1 are up-regulated, whereas Tcf711 is down-regulated. Normally, up-regulation of  $\beta$ -catenin expression would increase output of the pathway as measured by Tcf711 expression levels. However, up-regulation of Csnk2a1 negatively affects  $\beta$ -catenin-mediated output, which is reflected by Tcf711 being down-regulated in the module. Recently, we have studied US28-mediated activation

of  $\beta$ -catenin [46]. In that study, involvement of the upstream WNT/Frizzled pathway components activating  $\beta$ -catenin was ruled out and an alternative mechanism involving Rock1, which is also part of our module, was proposed. In the following we propose another mechanism for US28-mediated activation of  $\beta$ -catenin.

By hovering over Fgf7, Hgf and Figf, we could see that these proteins are enriched for the GO-term ‘growth factor activity’ (pink contour). These proteins are connected to  $\beta$ -catenin via Met. By requesting additional information, we can see that Met is a receptor tyrosine kinase. Using the plugin, a connection between Met and  $\beta$ -catenin is found via the KEGG pathway ‘Adherens junction’ (Fig. 10). Indeed, alternative mechanisms in the activation of  $\beta$ -catenin signaling involving release of  $\beta$ -catenin from cell-cell adherence junctions have been described (e.g. [50]). As US28 was also found to mediate cell migration [51, 52], loss of cell-cell contacts may explain increased levels of  $\beta$ -catenin signaling as observed in US28-expressing cells. When the observed increase of Hgf gene expression is reflected in increased excretion of this growth factor in US28-expressing cells, this may give rise to the following hypothesis explaining the enhanced TCF-LEF reporter gene activation in US28-expressing cells. Increased Hgf may activate the Met receptor tyrosine kinase in an auto- or paracrine fashion. The Met tyrosine kinase has been shown to mediate release of  $\beta$ -catenin from adherence junctions associated with the phosphorylation of  $\beta$ -catenin on tyrosine 654 [53, 54]. This phosphorylation may result in increased levels of  $\beta$ -catenin in the cytoplasm which could explain enhanced TCF-LEF activation. We are currently experimentally validating this hypothesis.



### Discussion

The case study demonstrates that our set-oriented visualization approach is well suited for analyzing protein modules enriched with gene expression data, Gene Ontology annotations, and KEGG pathway information. The visualization itself uses familiar visual concepts, such as node-link diagrams and contours drawn around items that belong to the same set, which makes interpretation intuitive. Our layout algorithm, based on SOMs, constructs an integrated layout of both network topology and set system topology. It allows for emphasizing either network topology or set system topology via a single parameter that is adjustable interactively by the user.

Existing approaches do not offer this flexibility, and will either optimize the layout of the set relations at the expense of the network topology or emphasize network topology to the detriment of the set system.

Other types of (network) visualization, such as adjacency matrices and enrichment tables, could also be used to integrate additional set data. However, these visualizations are not as intuitive and, more importantly, they are less effective in conveying the topology of the network and set system.

Scalability is a limitation of our approach: if the network is very large and if there are many sets, it is not possible to construct a comprehensive layout, which makes visual analysis ineffective. This is a natural limitation of any visualization approach based on node-link diagrams and set contours. Our technique relies on a focus and context approach, in which the network and set system should be pruned (computationally) down to the most relevant or significant components first. The resulting smaller network module(s) and set system can then be visually explored with our approach, and the domain expert can focus on the relevant details only to understand the underlying biology.

## Conclusions

We have proposed a set-oriented visual analysis approach for annotated network modules, where sets are shown as contours on top of a network node-link layout. We have implemented this approach in the Cytoscape app eXamine that enables the interactive exploration of annotated network modules. Subsequently, we have used the tool to re-analyze a data set that some of the co-authors have studied extensively. As a result of using the plugin, we have been able to formulate a new hypothesis about deregulated signaling of  $\beta$ -catenin by viral receptor proteins. This new hypothesis is currently being verified experimentally.

## Availability and Requirements

**Project name:** eXamine

**Project homepage:** <http://apps.cytoscape.org/apps/examine>

**Operating system(s):** all

**Programming language:** Java

**Other requirements:** Cytoscape 3.x

**License:** GPL2

**Any restrictions to use by non-academics:** None

### Competing interests

The authors declare that they have no competing interests.

### Author's contributions

KD, MEK, MAW and GWK conceived the visual analysis technique. KD and MEK implemented eXamine. CIB, MEK, GWK, MS and MJS applied it to the US28 case study. KD, MEK, MAW and GWK drafted the manuscript. All authors read and approved the final manuscript.

### Author details

<sup>1</sup>Eindhoven University of Technology, Den Dolech 2, 5600 MB, Eindhoven, The Netherlands. <sup>2</sup>Life Sciences, Centrum Wiskunde & Informatica (CWI), Science Park 123, 1098 XG, Amsterdam, The Netherlands. <sup>3</sup>VU University Amsterdam, De Boelelaan 1105, 1081 HV, Amsterdam, The Netherlands.

## References

1. Alizadeh, A.A., Eisen, M.B., Davis, R.E., Ma, C., Lossos, I.S., Rosenwald, A., Boldrick, J.C., Sabet, H., Tran, T., Yu, X., Powell, J.I., Yang, L., Marti, G.E., Moore, T., Hudson, J., Lu, L., Lewis, D.B., Tibshirani, R., Sherlock, G., Chan, W.C., Greiner, T.C., Weisenburger, D.D., Armitage, J.O., Warnke, R., Levy, R., Wilson, W., Grever, M.R., Byrd, J.C., Botstein, D., Brown, P.O., Staudt, L.M.: Distinct types of diffuse large B-cell lymphoma identified by gene expression profiling. *Nature* **403**(6769), 503–511 (2000)
2. Golub, T.R., Slonim, D.K., Tamayo, P., Huard, C., Gaasenbeek, M., Mesirov, J.P., Coller, H., Loh, M.L., Downing, J.R., Caligiuri, M.A.: Molecular classification of cancer: class discovery and class prediction by gene expression monitoring. *science* **286**(5439), 531–537 (1999)
3. van de Vijver, M.J., He, Y.D., van't Veer, L.J., Dai, H., Hart, A.A.M., Voskuil, D.W., Schreiber, G.J., Peterse, J.L., Roberts, C., Marton, M.J., Parrish, M., Atsma, D., Witteveen, A., Glas, A., Delahaye, L., van der Velde, T., Bartelink, H., Rodenhuis, S., Rutgers, E.T., Friend, S.H., Bernards, R.: A gene-expression signature as a predictor of survival in breast cancer. *The New England journal of medicine* **347**(25), 1999–2009 (2002)
4. Tarca, A.L., Draghici, S., Khatri, P., Hassan, S.S., Mittal, P., Kim, J.-s., Kim, C.J., Kusanovic, J.P., Romero, R.: A novel signaling pathway impact analysis. *Bioinformatics (Oxford, England)* **25**(1), 75–82 (2009)
5. Vaske, C.J., Benz, S.C., Sanborn, J.Z., Earl, D., Szeto, C., Zhu, J., Haussler, D., Stuart, J.M.: Inference of patient-specific pathway activities from multi-dimensional cancer genomics data using PARADIGM. *Bioinformatics (Oxford, England)* **26**(12), 237–245 (2010)
6. Ideker, T., Ozier, O., Schwikowski, B., Siegel, A.F.: Discovering regulatory and signalling circuits in molecular interaction networks. *Bioinformatics (Oxford, England)* **18**(Suppl 1), 233–240 (2002)
7. Dittrich, M.T., Klau, G.W., Rosenwald, A., Dandekar, T., Müller, T.: Identifying functional modules in protein-protein interaction networks: an integrated exact approach. *Bioinformatics* **24**(13), 223–231 (2008). doi:10.1093/bioinformatics/btn161
8. Kanehisa, M., Goto, S.: KEGG: Kyoto Encyclopedia of Genes and Genomes. *Nucleic Acids Research* **28**(1), 27–30 (2000)
9. Mitra, K., Carvunis, A.-R., Ramesh, S.K., Ideker, T.: Integrative approaches for finding modular structure in biological networks. *Nature Publishing Group* **14**(10), 719–732 (2013)
10. Ashburner, M., Ball, C.A., Blake, J.A., Botstein, D., Butler, H., Cherry, J.M., Davis, A.P., Dolinski, K., Dwight, S.S., Eppig, J.T., Harris, M.A., Hill, D.P., Issel-Tarver, L., Kasarskis, A., Lewis, S., Matese, J.C., Richardson, J.E., Ringwald, M., Rubin, G.M., Sherlock, G.: Gene ontology: tool for the unification of biology. *The Gene Ontology Consortium. Nature genetics* **25**(1), 25–29 (2000)
11. Gehlenborg, N., O'Donoghue, S.I., Baliga, N.S., Goesmann, A., Hibbs, M.A., Kitano, H., Kohlbacher, O., Neuweger, H., Schneider, R., Tenenbaum, D., Gavin, A.-C.: Visualization of omics data for systems biology. *Nature Methods* **7**(3s), 56–68 (2010)
12. Smooth, M.E., Ono, K., Ruschewski, J., Wang, P.L., Ideker, T.: Cytoscape 2.8: new features for data integration and network visualization. *Bioinformatics* **27**(3), 431–432 (2011)
13. van Iersel, M.P., Kelder, T., Pico, A.R., Hanspers, K., Coort, S., Conklin, B.R., Evelo, C.: Presenting and exploring biological pathways with PathVisio. *BMC Bioinformatics* **9**(1), 399 (2008)
14. Bertault, F., Eades, P.: Drawing hypergraphs in the subset standard. In: *Proc. 8th Int. Symp. on Graph Drawing. Lecture Notes in Computer Science*. Springer, Berlin, Heidelberg
15. Simonetto, P., Auber, D., Archambault, D.: Fully automatic visualisation of overlapping sets. *Computer Graphics Forum* **28**(3), 967–974 (2009)
16. Riche, N.H., Dwyer, T.: Untangling Euler diagrams. *IEEE Transactions on Visualization and Computer Graphics* **16**(6), 1090–1099 (2010)
17. Alper, B., Riche, N., Ramos, G., Czerwinski, M.: Design study of LineSets, a novel set visualization technique. *IEEE Transactions on Visualization and Computer Graphics* **17**(12), 2259–2267 (2011)
18. Dinkla, K., van Kreveld, M.J., Speckmann, B., Westenberg, M.A.: Kelp diagrams: Point set membership visualization. *Computer Graphics Forum* **31**(3), 875–884 (2012)
19. Collins, C., Penn, G., Carpendale, S.: Bubble Sets: Revealing set relations with isocontours over existing visualizations. *IEEE Transactions on Visualization and Computer Graphics* **15**(6), 1009–1016 (2009)
20. Smith, A.M., Xu, W., Sun, Y., Faeder, J.R., Marai, G.E.: Rulebender: integrated modeling, simulation and visualization for rule-based intracellular biochemistry. *BMC bioinformatics* **13**(Suppl 8), 3 (2012)
21. Meulemans, W., Riche, N.H., Speckmann, B., Alper, B., Dwyer, T.: KelpFusion: A hybrid set visualization technique. *IEEE Trans. Visualization and Computer Graphics* **19**(11), 1846–1858 (2013)
22. Sugiyama, K., Misue, K.: Visualization of structural information: automatic drawing of compound digraphs. *Systems, Man and Cybernetics, IEEE Transactions on* **21**(4), 876–892 (1991)
23. Shneiderman, B., Aris, A.: Network visualization by semantic substrates. *Visualization and Computer Graphics, IEEE Transactions on* **12**(5), 733–740 (2006)
24. Barsky, A., Munzner, T., Gardy, J., Kincaid, R.: Cerebral: Visualizing multiple experimental conditions on a graph with biological context. *IEEE Transactions on Visualization and Computer Graphics* **14**(6), 1253–1260 (2008)
25. Kohonen, T.: The self-organizing map. *Proceedings of the IEEE* **78**(9), 1464–1480 (1990)
26. Meyer, B.: Self-organizing graphs—a neural network perspective of graph layout. In: *Graph Drawing*, pp. 246–262 (1998). Springer
27. Fruchterman, T.M.J., Reingold, E.M.: Graph drawing by force-directed placement. *Software: Practice and Experience* **21**(11), 1129–1164 (1991)
28. Dwyer, T., Marriott, K., Stuckey, P.J.: Fast node overlap removal. In: *Graph Drawing. Lecture Notes in Computer Science*, vol. 3843, pp. 153–164 (2006)
29. Vesanto, J.: SOM-based data visualization methods. *Intelligent Data Analysis* **3**(2), 111–126 (1999)
30. MacCallum, R., Redmond, S., Christophides, G.: An expression map for anopheles gambiae. *BMC Genomics* **12**(1), 620 (2011)

31. de Berg, M., Cheong, O., van Kreveld, M., Overmars, M.: Computational Geometry: Algorithms and Applications. Springer, Berlin, Heidelberg (2008)
32. Holten, D., van Wijk, J.J.: Force-directed edge bundling for graph visualization. *Computer Graphics Forum* **28**(3), 983–990 (2009)
33. Shepard, D.: A two-dimensional interpolation function for irregularly-spaced data. In: Proceedings of the 1968 23rd ACM National Conference. ACM '68, pp. 517–524. ACM, New York, NY, USA (1968). doi:[10.1145/800186.810616](https://doi.org/10.1145/800186.810616). <http://doi.acm.org/10.1145/800186.810616>
34. Vivid Solutions: Java Topology Suite (2003)
35. Harrower, M., Brewer, C.A.: ColorBrewer.org: An Online Tool for Selecting Colour Schemes for Maps. John Wiley & Sons, Ltd, Chichester, UK
36. Gandhi, M.K., Khanna, R.: Human cytomegalovirus: clinical aspects, immune regulation, and emerging treatments. *The Lancet Infectious Diseases* **4**(12), 725–738 (2004). doi:[10.1016/S1473-3099\(04\)01202-2](https://doi.org/10.1016/S1473-3099(04)01202-2)
37. Söderberg-Nauclér, C.: Does cytomegalovirus play a causative role in the development of various inflammatory diseases and cancer? *Journal of Internal Medicine* **259**(3), 219–246 (2006). doi:[10.1111/j.1365-2796.2006.01618.x](https://doi.org/10.1111/j.1365-2796.2006.01618.x)
38. Cobbs, C.S., Harkins, L., Samanta, M., Gillespie, G.Y., Bharara, S., King, P.H., Nabors, L.B., Cobbs, C.G., Britt, W.J.: Human cytomegalovirus infection and expression in human malignant glioma. *Cancer Research* **62**(12), 3347–3350 (2002). <http://cancerres.aacrjournals.org/content/62/12/3347.full.pdf+html>
39. Harkins, L., Volk, A.L., Samanta, M., Mikolaenko, I., Britt, W.J., Bland, K.I., Cobbs, C.S.: Specific localisation of human cytomegalovirus nucleic acids and proteins in human colorectal cancer. *The Lancet* **360**(9345), 1557–1563 (2002). doi:[10.1016/S0140-6736\(02\)11524-8](https://doi.org/10.1016/S0140-6736(02)11524-8)
40. Cinatl J, Jr., JU, V., R, K., H, W.D.: Oncomodulatory signals by regulatory proteins encoded by human cytomegalovirus: a novel role for viral infection in tumor progression. *FEMS Microbiol Rev* **28**, 59–77 (2004)
41. Randolph-Habecker, J., Rahill, B., Torok-Storb, B., Vieira, J., Kolattukudy, P.E., Rovin, B.H., Sedmak, D.D.: The expression of the cytomegalovirus chemokine receptor homolog US28 sequesters biologically active CC chemokines and alters IL-8 production. *Cytokine* **19**(1), 37–46 (2002)
42. Casarosa, P., Bakker, R.A., Verzijl, D., Navis, M., Timmerman, H., Leurs, R., Smit, M.J.: Constitutive signaling of the human cytomegalovirus-encoded chemokine receptor US28. *Journal of Biological Chemistry* **276**(2), 1133–1137 (2001). doi:[10.1074/jbc.M008965200](https://doi.org/10.1074/jbc.M008965200). <http://www.jbc.org/content/276/2/1133.full.pdf+html>
43. Maussang, D., Verzijl, D., van Walsum, M., Leurs, R., Holl, J., Pleskoff, O., Michel, D., van Dongen, G.A.M.S., Smit, M.J.: Human cytomegalovirus-encoded chemokine receptor US28 promotes tumorigenesis. *Proceedings of the National Academy of Sciences* **103**(35), 13068–13073 (2006). doi:[10.1073/pnas.0604433103](https://doi.org/10.1073/pnas.0604433103). <http://www.pnas.org/content/103/35/13068.full.pdf+html>
44. Maussang, D., Langemeijer, E., Fitzsimons, C.P., Stigter-van Walsum, M., Dijkman, R., Borg, M.K., Slinger, E., Schreiber, A., Michel, D., Tensen, C.P., van Dongen, G.A.M.S., Leurs, R., Smit, M.J.: The human cytomegalovirus-encoded chemokine receptor US28 promotes angiogenesis and tumor formation via cyclooxygenase-2. *Cancer Research* **69**(7), 2861–2869 (2009). doi:[10.1158/0008-5472.CAN-08-2487](https://doi.org/10.1158/0008-5472.CAN-08-2487). <http://cancerres.aacrjournals.org/content/69/7/2861.full.pdf+html>
45. Slinger, E., Maussang, D., Schreiber, A., Siderius, M., Rahbar, A., Fraile-Ramos, A., Lira, S.A., Soderberg-Naucler, C., Smit, M.J.: HCMV-encoded chemokine receptor US28 mediates proliferative signaling through the IL-6-STAT3 axis. *Sci. Signal.* **3**(133), 58 (2010). doi:[10.1126/scisignal.2001180](https://doi.org/10.1126/scisignal.2001180). <http://stke.sciencemag.org/cgi/reprint/sigtrans;3/133/ra58.pdf>
46. Langemeijer, E.V., Slinger, E., de Munnik, S., Schreiber, A., Maussang, D., Vischer, H., Verkaar, F., Leurs, R., Siderius, M., Smit, M.J.: Constitutive  $\beta$ -catenin signaling by the viral chemokine receptor US28. *PLoS ONE* **7**(11), 48935 (2012). doi:[10.1371/journal.pone.0048935](https://doi.org/10.1371/journal.pone.0048935)
47. Gautier, L., Cope, L., Bolstad, B.M., Irizarry, R.A.: affy—analysis of affymetrix genechip data at the probe level. *Bioinformatics* **20**(3), 307–315 (2004). doi:[10.1093/bioinformatics/btg405](https://doi.org/10.1093/bioinformatics/btg405)
48. Smyth, G.K.: Limma: linear models for microarray data. In: Gentleman, R., Carey, V., Dudoit, S., Irizarry, R., Huber, W. (eds.) *Bioinformatics and Computational Biology Solutions Using R and Bioconductor*, pp. 397–420. Springer, New York (2005)
49. Minisini, R., Tulone, C., Lüske, A., Michel, D., Mertens, T., Gierschik, P., Moepps, B.: Constitutive inositol phosphate formation in cytomegalovirus-infected human fibroblasts is due to expression of the chemokine receptor homologue pUS28. *Journal of Virology* **77**(8), 4489–4501 (2003). <http://jvi.asm.org/content/77/8/4489.full.pdf+html>
50. Zhurinsky, J., Shutman, M., Ben-Ze'ev, A.: Differential mechanisms of LEF/TCF family-dependent transcriptional activation by  $\beta$ -catenin and plakoglobin. *Molecular and Cellular Biology* **20**(12), 4238–4252 (2000). doi:[10.1128/MCB.20.12.4238-4252.2000](https://doi.org/10.1128/MCB.20.12.4238-4252.2000). <http://mcb.asm.org/content/20/12/4238.full.pdf+html>
51. Strebblow, D.N., Soderberg-Naucler, C., Vieira, J., Smith, P., Wakabayashi, E., Ruchti, F., Mattison, K., Altschuler, Y., Nelson, J.A.: The human cytomegalovirus chemokine receptor US28 mediates vascular smooth muscle cell migration. *Cell* **99**(5), 511–520 (1999). doi:[10.1016/S0092-8674\(00\)81539-1](https://doi.org/10.1016/S0092-8674(00)81539-1)
52. Strebblow, D.N., Vomaske, J., Smith, P., Melnychuk, R., Hall, L., Pancheva, D., Smit, M., Casarosa, P., Schlaepfer, D.D., Nelson, J.A.: Human cytomegalovirus chemokine receptor US28-induced smooth muscle cell migration is mediated by focal adhesion kinase and Src. *Journal of Biological Chemistry* **278**(50), 50456–50465 (2003). doi:[10.1074/jbc.M307936200](https://doi.org/10.1074/jbc.M307936200). <http://www.jbc.org/content/278/50/50456.full.pdf+html>
53. Herynk, M.H., Tsan, R., Radinsky, R., Gallick, G.E.: Activation of c-Met in colorectal carcinoma cells leads to constitutive association of tyrosine-phosphorylated  $\beta$ -catenin. *Clinical & Experimental Metastasis* **20**(4), 291–300 (2003). doi:[10.1023/A:1024024218529](https://doi.org/10.1023/A:1024024218529)
54. Purcell, R., Childs, M., Maibach, R., Miles, C., Turner, C., Zimmermann, A., Sullivan, M.: HGF/c-Met related activation of beta-catenin in hepatoblastoma. *Journal of Experimental & Clinical Cancer Research* **30**(1), 96 (2011). doi:[10.1186/1756-9966-30-96](https://doi.org/10.1186/1756-9966-30-96)